Supporting Information

Attachment of Pathogenic Prion Protein to Model Oxide Surfaces

Kurt H. Jacobson[1], Thomas R. Kuech[2] and Joel A. Pedersen[1,2,3,*]
[1] Department of Civil and Environmental Engineering, [2] Environmental Chemistry and Technology Program, [3] Department of Soil Science, University of Wisconsin, Madison, WI 53706

*Corresponding author address: Department of Soil Science, University of Wisconsin, 1525 Observatory Drive, Madison, WI 53706-1299; phone: (608) 263-4971; fax: (608) 265-2595; e-mail: joelpedersen@wisc.edu

SUPPLEMENTAL MATERIALS AND METHODS

Total Protein Assay. To obtain the most accurate protein concentration for the purified PrP preparations, we modified the bicinchoninic acid dye binding assay (Pierce Cat #23225, Rockford, IL) to maximize access of bicinchoninic acid to the protein backbone of PrP by denaturing the PrP fibrils prior to the reaction. To accomplish this, all PrP^{TSE} samples, bovine serum albumin (BSA) standards (>99% pure, Sigma Aldrich, St. Louis, MO), and recombinant PrP (recPrP) standards (>95% pure, Jena Biosciences, Jena, Germany) were heated for 10 min at 99 °C in 3.2% SDS, sonicated for 1 min at 750 W (GE750 cuphorn ultrasonicator, Sonics and Materials, Newtown, CT) before being heated for an additional 5 min at 99 °C. After cooling, the protein solutions were subjected to the assay as recommended by the manufacturer. Absorbance at 562 nm of the standards and unknowns was then measured with a BioTek Epoch Microplate Reader (Winooski, VT). The protein concentrations in quadruplicate samples of each pathogenic prion protein preparation were quantified against the BSA and recPrP standard curves. Both standard curves yielded the same estimate of protein concentration in the prion protein preparations.

Purity of Purified Prion Preparations. The purities of the PrP^{TSE} and $PrP^{27\text{-}30}$ preparations described in the main text were determined by immunoblotting and silver staining of SDS-PAGE separated samples using methods described previously.[1] Figure S1 displays an exemplary immunoblot and SDS-PAGE gel.

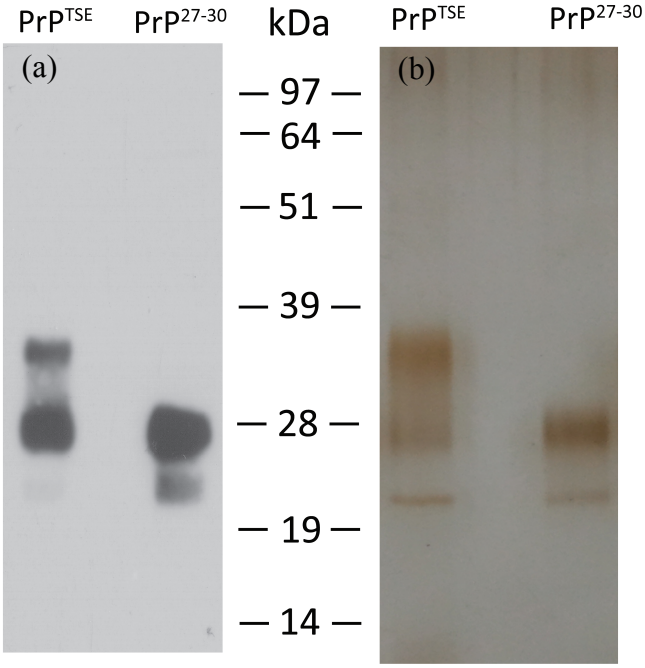

Figure S1. Purified PrP^{TSE} and $PrP^{27\text{-}30}$ preparations subjected to (a) immunoblotting with monoclonal anti-PrP antibody 3F4 (Covance, Princeton, NJ) and (b) SDS-PAGE with silver staining (Pierce Silver Stain Kit, Rockford, IL). The immunoblot shows the relative molecular mass distribution of PrP molecules present in the purified PrP preparations. Note the presence of the mature PrP monomer (~35 kDa) in the PrP^{TSE} preparation (thermolysin-treated) and its absence in the $PrP^{27\text{-}30}$ preparation (proteinase K-treated). The large band at ~28 kDa is the di-glycosylated, N-terminally truncated PrP molecule. The fainter band at ~24 kDa is the mono-glycosylated, N-terminally truncated PrP molecule. The silver stained gel shows both the molecular mass distributions of PrP for the two preparations and the high purity of PrP obtained using these methods. The concentration of the only resolvable contaminant, the heavy chain of ferritin (~21 kDa), was determined, by densitometry, to be ≤ 5% of the silver stainable material in all purifications. We note that, glycoproteins such as PrP stain weakly with silver compared to un-glycosylated proteins.

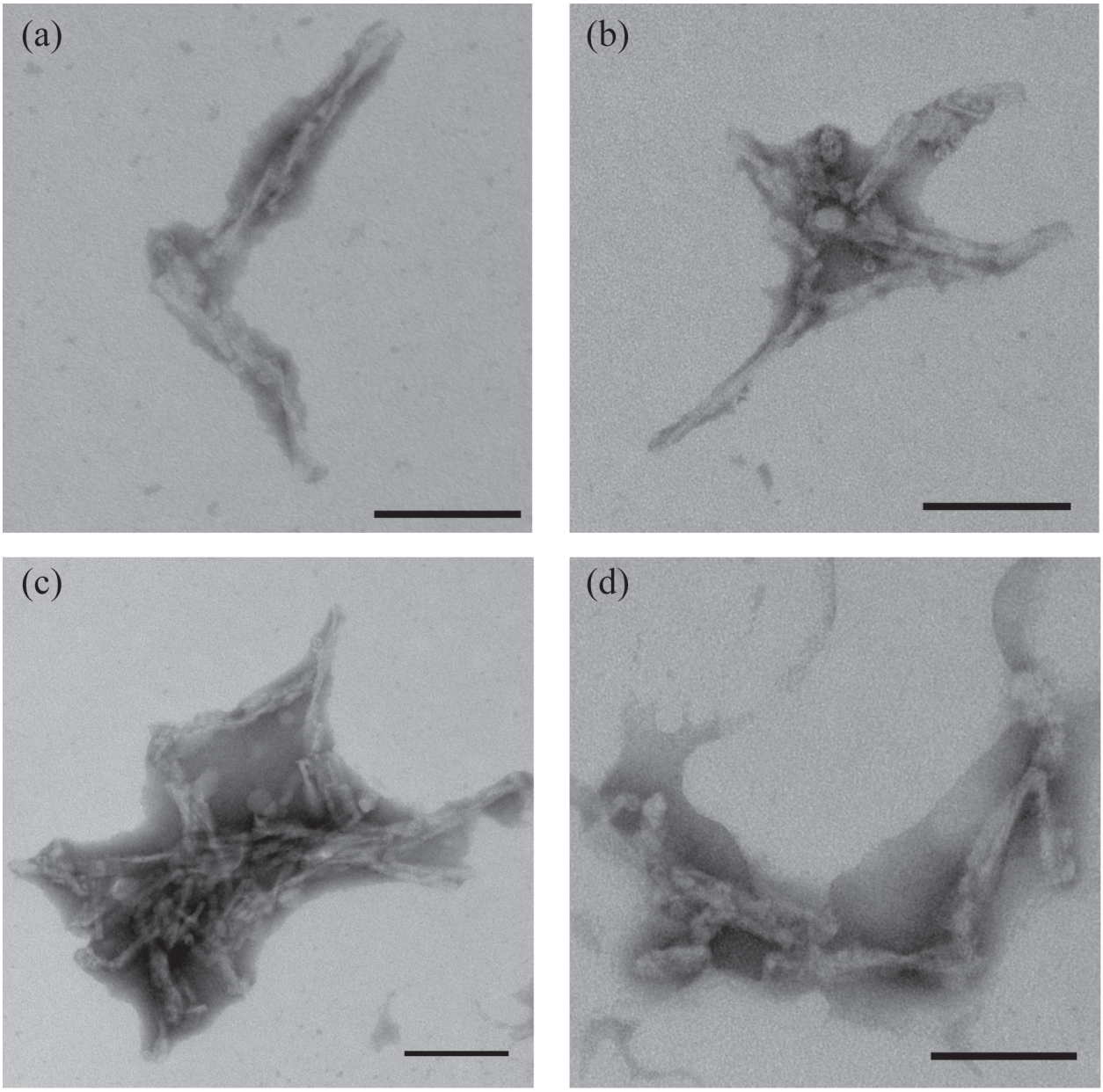

Figure S2. Transmission Electron Micrographs of Purified Prion Fibrils Representative transmission electron micrographs of $PrP^{27\text{-}30}$ (a and b) and PrP^{TSE} (c and d). Black bars are 100 nm. The ~12 nm diameter annular structures are ferritin 24-mers that co-purify with PrP fibrils. Purified preparations were diluted 1 to 100 in ultrapure water, coated on to carbon grids, negatively stained with methylamine tungstate and dried. Images were collected using a Philips CM120 (Amsterdam, The Netherlands) operating at 80 keV.

Estimation of the Point of Zero Charge of Al_2O_3-coated Sensors. The point of zero charge (pH_{pzc}) of the Al_2O_3 surface coatings was estimated by measuring the attachment of citrate-coated TiO_2 nanoparticles to Al_2O_3–coated QCM-D sensors as a function of pH. Over the tested pH range (6.5-8), the citrate-TiO_2 nanoparticles exhibit a negative ζ-potential ($\zeta = -26$ to -30 mV). The TiO_2 nanoparticles were suspended in 3 mM HEPES solutions at pH 6.5, 6.75, 7.0, 7.25, 7.5, 7.75, and 8.0 with *I* adjusted to 5 mM wth NaCl. Attachment of nanoparticles at or near their diffusion-limited rate was observed at tested pH values ≤7.50. At pH values of 7.75 and 8.00, no attachment was observed. These data indicate that the pH_{pzc} of the Al_2O_3 surfaces used are between 7.50 and 7.75.

QCM-D Sensor and Flow Chamber Cleaning Procedure. The following cleaning procedure was used immediately after each QCM-D experiment:

(1) With the experiment sensors still in the flow cells, 2% (v/v) LpH (Steris, Mentor, OH) was pumped through the chamber for 20 min at 100 $\mu L \cdot min^{-1.}$
(2) A 2% (w/v) solution of sodium dodecylsulfate (SDS) was pumped (flow rate 100 $\mu L \cdot min^{-1}$) for 20 min.
(3) The flow cells and experimental sensors were rinsed with ultrapure water (18 MΩ·cm; Barnstead NANOpure Ultrapure Water System, Dubuque, Iowa) at a flow rate of 100 $\mu L \cdot min^{-1}$ for 10 min.
(4) Following briefly pumping air through the flow cells to remove most liquid, the experimental sensors were removed from the flow cells and transferred to a polytetrafluoroethylene holder.
(5) The experimental sensors were sonicated for 20 min in a 2% (w/v) SDS solution (Branson 2510 sonic bath, Danbury, CT).
(6) Following sonication, the experimental sensors were rinsed sequentially with ultrapure water, 2-propanol, and ultrapure water.
(7) After drying under flowing Ultra-High Purity N_2 gas, the sensors were placed in a UV/ozone chamber (Prochamber, Bioforce Nanosciences, Ames, Iowa) for 15 min cleaning.
(8) After removal of the sensors from the flow chambers, Au-coated QCM-D sensors were sealed in the flow chambers.
(9) Cobas Cleaner solution (Roche, Basel, Switzerland) was pumped through the cells for 10 min (200 $\mu L \cdot min^{-1}$).
(10) 2% (v/v) Hellmanex II (Hellma GmbH, Müllheim, Germany) was then pumped through the cells for 10 min (200 $\mu L \cdot min^{-1}$).
(11) Ultrapure water was pumped through the flow cells for 30 min (200 $\mu L \cdot min^{-1}$).
(12) Following briefly pumping air through the flow cells to remove bulk water, the Au-coated sensors were removed and the flow cells were blown dry using N_2 gas.

Immediately prior to use the QCM-D sensors were cleaned using the following procedure:

(1) The sensors were sequentially rinsed with ultrapure water, 2-propanol, and ultrapure water.
(2) Following drying under flowing N_2 gas, the sensors were cleaned in a UV/ozone chamber for 15 min.

Locally Weighted Scatterplot Smoothing (LOESS) of QCM-D Data. To remove the influence of normal variation in recorded frequencies caused by instrument drift from calculated initial attachment rates, all QCM-D data were subjected to Locally Weighted Scatterplot Smoothing (LOESS) with a smoothing parameter of 0.1.[2] LOESS fits a low, variable-order polynomial (between first and second) to the data over a small range, which is controlled by the value of the smoothing parameter, using a weighted least squares procedure. Although smoothing parameter values between 0.25 and 0.50 are suggested for most applications, the high temporal resolution of the QCM-D data collected in this study (2-5 Δf measurements per s) allowed use of a value of 0.1 Use of a small smoothing parameter prevented oversmoothing of the frequency curve that could have obscured small, yet significant, variations of the data.

Determination of minimum discernible attachment efficiency. To determine the smallest calculated efficiency (α) that could be regularly differentiated from background QCM-D signal drift, the slope of the LOESS smoothed $\Delta f_5/5$ curve was calculated for the 10 minutes of data immediately prior to the introduction of protein to the flow chamber. These slopes were then divided by the slope of the protein attachment curve to a PLL surface using Eq. 2 to calculate a theoretical α of the background noise for each run. The largest of these slopes (0.0019) was the assigned as the lowest discernible attachment efficiency.

Refractive Index of Buffers. The refractive indices of buffers used in OWLS experiments was measured using a Rudolph Research Model J157-633 Refractometer (Hackettstown, NJ) at λ = 632.8 nm and 24.0 °C (Table S1). Briefly, 800 μL of the sample solution was pipetted onto the measurement crystal, the temperature was allowed to equilibrate for 2 min, and 100 replicate measurements were performed. Following data acquisition, the sample area was cleaned with by sequential rinses of ultrapure water, 2-propanol, and ultrapure water before being allowed to air dry.

Table S1. Refractive Indices (n_c) at λ = 632.8 nm of Buffers Used in OWLS Experiments

pH	Buffer	I (mM)	n_c	Std. Dev.
6	MES	5	1.33200	0.00003
		50	1.33257	0.00002
7	HEPES	5	1.33199	0.00003
		50	1.33254	0.00002
8	HEPES	5	1.33198	0.00003
		50	1.33256	0.00002
9	CHES	5	1.33203	0.00003
		50	1.33251	0.00003

OWLS Waveguide and Flow Chamber Cleaning Procedure. The following cleaning procedure was used immediately after each OWLS experiment:

(1) With the experiment waveguide still in the flow cell, 2% (v/v) LpH was pumped through the chamber for 20 min at 100 $\mu L \cdot min^{-1.}$
(2) Cobas Cleaner solution was pumped through the flow cell (flow rate 100 $\mu L \cdot min^{-1}$) for 20 min.
(3) Ultrapure water was pumped through the flow cell (flow rate 100 $\mu L \cdot min^{-1}$) for 20 min.
(4) Following briefly pumping air through the flow cell to remove most liquid, the waveguide was removed from the flow cells and transferred to a 2 mL microcentrifuge tube.
(5) The microcentrifuge tube containing the waveguide was filled with Cobas Cleaner solution and sonicated for 15 min.
(6) After sonication, the waveguide was rinsed sequentially with ultrapure water, 2-propanol, and ultrapure water.
(7) The waveguide was dried under flowing N_2 gas and placed in a UV/ozone chamber for 15 min cleaning.
(8) Following removal of the waveguide, the Viton O-ring was separated from the body and both were placed in a beaker filled with 2-propanol and sonicated for 15 min.
(9) After sonication, the Viton O-ring and flow cell body were rinsed in ultrapure water and dried under flowing N_2.

Immediately prior to use the OWLS sensors cleaned using the following procedure:

(1) The sensors were sequentially rinsed with ultrapure water, 2-propanol, and ultrapure water.
(2) Following drying under flowing N_2 gas, the sensors were cleaned in a UV/ozone chamber for 15 min.

Atomic Force Microscopy (AFM). AFM images were acquired in tapping mode in solution using a fluid cell (MTFML, Bruker) with 120 μm oxide-sharpened silicon nitride V-shaped cantilevers (model DNP-S, nominal spring constant = 0.24 $N \cdot m^{-1}$). Drive frequencies were between 9.26 and 9.41 kHz. Drive amplitudes ranged from 644 to 932 mV. Samples were attached to the AFM puck with double stick tape. A small drop of MES buffer (pH 6, I = 5mM) was placed on the top surface of the sample prior to assembling the liquid cell. Each sample was imaged at a minimum of three random locations using the model EV scanner (Bruker) operating at 2 Hz and collecting 256 data points per line over a nominal maximum scan range of 12 μm × 12 μm. Root mean squared roughness (R_{RMS}) of selected areas was calculated using the following formula in the Nanoscope Analysis software:

SUPPLEMENTAL RESULTS AND DISCUSSION

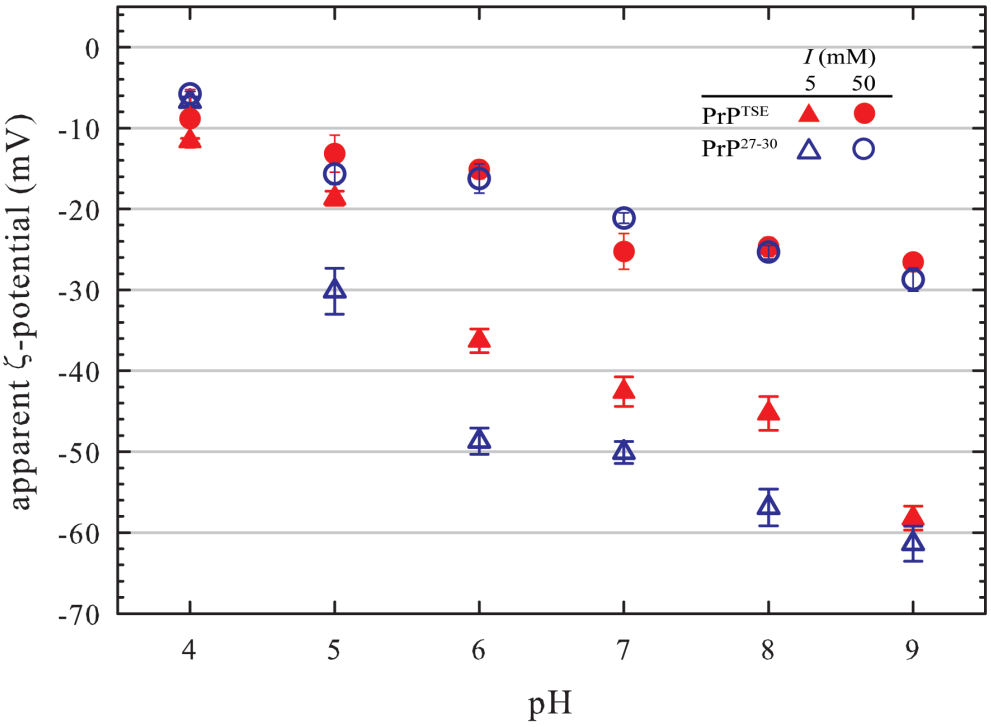

Figure S3. Apparent ζ-potentials of purified prion proteins. To provide a point of reference for comparison with previous studies, we calculated apparent ζ-potentials of purified prion protein fibrils assuming they possess a regular cylindrical geometry with a radius of 6 nm and a random orientation to the electric field (Eq. S1).[3] We emphasize however, that purified pathogenic prion protein does likely not exist in solution as individual regularly cylindrical fibrils (see Fig S2). To our knowledge, no analysis method exists to accurately account for the heterogeneity of prion fibril structure in converting μ_e values to ζ-potentials.

$$\zeta_{cyl} = \frac{3\eta \cdot \mu_e}{\varepsilon_r \varepsilon_0 (1+2f(\kappa r))} \qquad \text{(S1)}$$

Where η is the dynamic viscosity (Pa·s), μ_e is the measured average electrophoretic mobility ($m^2 \cdot V^{-1} \cdot s^{-1}$), ε_r is the relative permittivity of water (-), ε_0 is the permittivity of free space ($F \cdot m^{-1}$) and $f(\kappa r)$ is defined as:

$$f(kr) = \frac{1}{2}\left(1 + \frac{1}{\left(1+\frac{2.55}{(\kappa r[1+e^{(-\kappa r)}])}\right)^2}\right) \qquad \text{(S2)}$$

Where κ is the inverse Debye length (m^{-1}) and r is the radius of the cylinders (m^{-1})

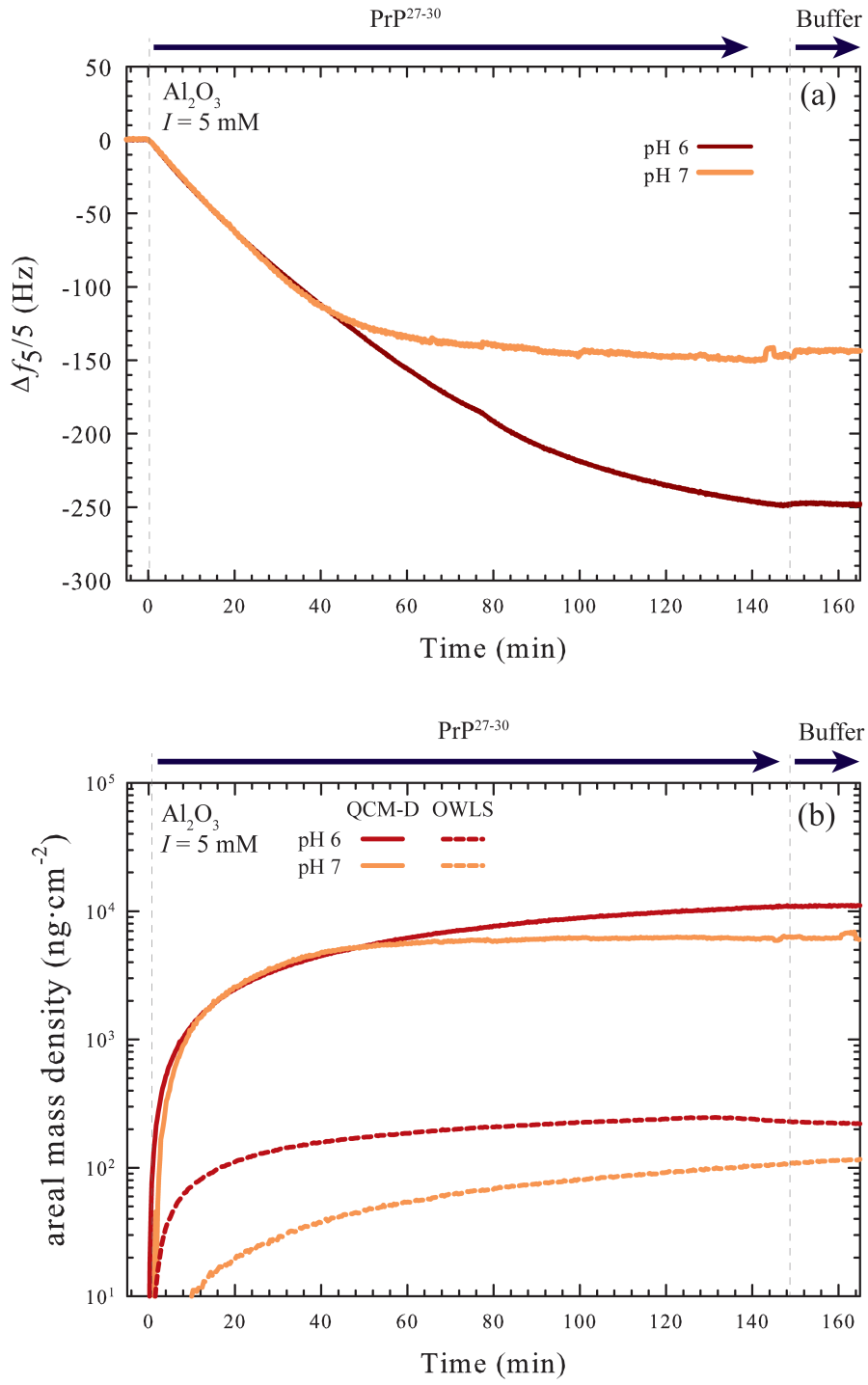

Figure S4. Fully formed PrP^{27-30} adlayers on Al_2O_3. (a) The QCM-D recorded $\Delta f_5/5$ values of PrP^{27-30} attaching to Al_2O_3 at pH 6 and 7, I = 5 mM. (b) The Kelvin-Voight modeled and OWLS sensed areal mass densities of fully formed protein adlayers on Al_2O_3 surfaces. The large difference in areal mass densities sensed by both methods is caused by the large fraction of water (~98%) that is acoustically coupled to the adlayer. The dashed grey lines and arrows above the plots indicate the solution conditions over time.

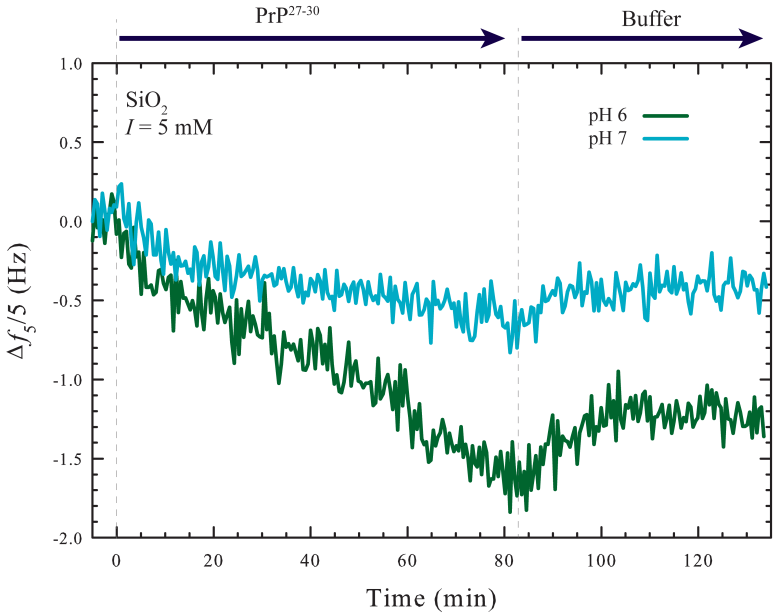

Figure S5. Fully formed PrP$^{27\text{-}30}$ adlayers on SiO_2. The QCM-D recorded $\Delta f_5/5$ values of PrP$^{27\text{-}30}$ attaching to SiO_2 at pH 6 and 7, I = 5 mM. The small frequency changes suggest that the adlayers present on SiO_2 are not laterally homogeneous and thus not amenable to Kelvin-Voight viscoelastic modeling. In Figure 4 (attachment to Al_2O_3), the t = 5 min time point produced a larger $\Delta f_5/5$ (−17 Hz) but did not produce a laterally homogeneous adlayer. The dashed grey lines and arrows above the plots indicate the solution conditions over time.

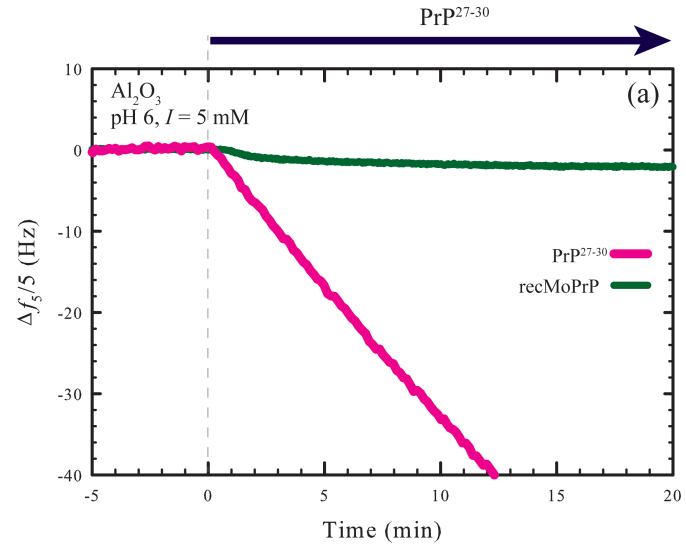
PrP27-30
Al2O3
pH 6, I = 5 mM
(a)
PrP27-30
recMoPrP
Δf5/5 (Hz)
Time (min)

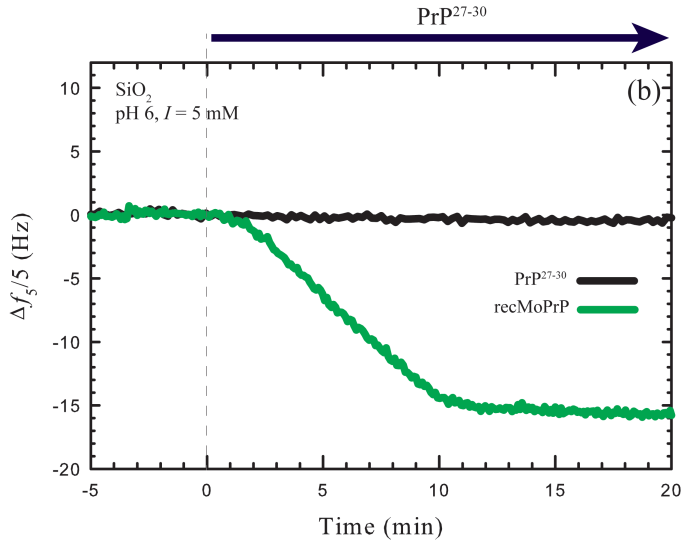
PrP27-30
SiO2
pH 6, I = 5 mM
(b)
PrP27-30
recMoPrP
Δf5/5 (Hz)
Time (min)

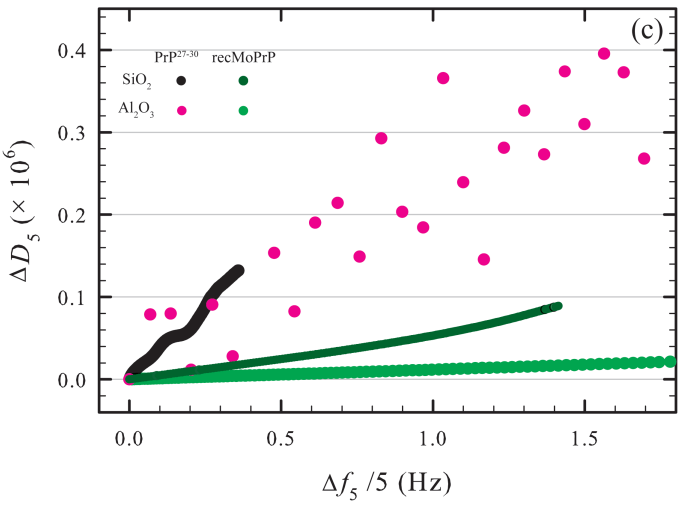
(c)
PrP27-30
recMoPrP
SiO2
Al2O3
ΔD5 (× 10^6)
Δf5 /5 (Hz)

Figure S6. Frequency and dissipation plots for the attachment of PrP^{27-30} and recMoPrP to Al_2O_3 and SiO_2. To compare the structural properties of infectious and recombinantly expressed prion protein adlayers coated on (a) Al_2O_3 and (b) SiO_2 surfaces, the Δf data at a single solution condition (pH 6, I = 5 mM) are plotted. Prokaryotically expressed mouse PrP (recMoPrP; 95% sequence homology to hamster PrP^{27-30})[4] carries a net positive charge at this pH, does not aggregate, and attached readily to (b) SiO_2 but not to (a) Al_2O_3. PrP^{27-30} attaches efficiently to Al_2O_3 and not SiO_2. (c) Plotting the observed ΔD versus Δf for each of these attachment experiments shows the marked differences between recMoPrP and *bona fide* PrP fibrils. Adlayers composed of recMoPrP show very low dissipation relative to change in frequency, suggesting the protein couples the vibrations of the QCM-D sensor efficiently. Attachment of *bona fide* PrP fibrils to both SiO_2 and Al_2O_3 produce curves of markedly steeper slopes, implying much less vibrational coupling. While the mass of PrP^{27-30} attached to the two oxides differed dramatically, as evidenced by the final Δf observed at the conclusion of the experiment, the slopes of these plots suggest the structural properties of the material attached was similar.

Table S3. Initial Attachment Rates (k_{QCM-D}) and Attachment Efficiencies (α) for PrP^{TSE}. Estimated from QCM-D Data.

surface	pH	*I* (mM)	k_{QCM-D} (Hz·min^{-1})	α (-)
Al_2O_3	6	5	2.29 (0.03)	1.06 (0.01)
		50	0.17 (0.01)	1.61 (0.1)
	7	5	2.98 (0.14)	1.10 (0.05)
		50	0.55 (0.07)	1.24 (0.15)
	8	5	0.14 (0.02)	0.05 (0.01)
		50	0.83 (0.09)	1.07 (0.11)
	9	5	0.27 (0.01)	0.10 (0.00)
		50	1.50 (0.05)	0.94 (0.03)
SiO_2	6	5	0.007 (0.002)	0.01 (0.01)
		50	0.03 (0.01)	0.29 (0.080)
	7	5	0.03 (0.01)	0.011 (0.01)
		50	0.04 (0.006)	0.11 (0.03)
	8	5	0.006 (0.001)	0.002 (0.001)
		50	0.015 (0.001)	0.020 (0.001)
	9	5	0.005 (0.004)	0.002 (0.001)
		50	0.028 (0.008)	0.017 (0.002)
PLL	6	5	2.17 (0.1)	
		50	0.10 (0.01)	
	7	5	2.71 (0.06)	
		50	0.43 (0.067)	
	8	5	2.71 (0.14)	
		50	0.77 (0.14)	
	9	5	2.80 (0.08)	
		50	1.60 (0.02)	

Table S4. Initial Attachment Rates (k_{QCM-D}) and Attachment Efficiencies (α) for PrP^{27-30} calculated from QCM-D Data.

surface	pH	*I* (mM)	k_{QCM-D} (Hz·min^{-1})	α (-)
Al_2O_3	6	5	3.94 (0.11)	1.02 (0.03)
		50	0.58 (0.03)	1.52 (0.08)
	7	5	2.54 (0.06)	0.89 (0.07)
		50	0.54 (0.04)	1.01 (0.06)
	8	5	0.15 (0.08)	0.04 (0.02)
		50	1.21 (0.06)	0.64 (0.03)
	9	5	0.14 (0.01)	0.04 (0.01)
		50	1.00 (0.07)	0.44 (0.12)
SiO_2	6	5	0.11 (0.01)	0.03 (0.01)
		50	0.10 (0.01)	0.27 (0.07)
	7	5	0.10 (0.03)	0.03 (0.03)
		50	0.02 (0.02)	0.04 (0.01)
	8	5	0.14 (0.01)	0.04 (0.01)
		50	0.08 (0.02)	0.04 (0.01)
	9	5	0.03 (0.02)	0.01 (0.01)
		50	0.01 (0.01)	0.01 (0.01)
PLL	6	5	3.85 (0.09)	
		50	0.38 (0.03)	
	7	5	3.94 (0.22)	
		50	0.54 (0.03)	
	8	5	3.51 (0.19)	
		50	1.89 (0.07)	
	9	5	3.96 (0.11)	
		50	2.27 (0.06)	

References

(1) Jacobson, K.H.; Lee, S.; Somerville, R.A.; McKenzie, D.; Benson, C.H.; Pedersen, J.A. Pathogenic prion protein transport through soils. *J. Environ. Qual.* **2010**, *39*, 1145-1152

(2) Cleveland, W.S.; Devlin, S.T. Locally weighted regression: An approach to regression analysis by local fitting. *J. Am. Stat. Assoc.* **1988**, *83*, 596-610.

(3) Ohshima, H. Henry's function for electrophoresis of a cylindrical colloidal particle. *J. Coll. Interf. Sci.* **1996**, *180*, 299-301.

(4) Wopfner, F.; Weidenhöfer, G.; Schneider, R.; von Brunn, A.; Gilch, S.; Schwarz, T.F.; Werner, T.; Schätzl, H.M. Analysis of 27 mammalian and 9 avian PrPs reveals high conservation of flexible regions of the prion protein. *J. Mol. Bio.* **1999**, 1163-1178.